

DESY-06-015
February 2006

Measurement of high- Q^2 deep inelastic scattering cross sections with a longitudinally polarised positron beam at HERA

ZEUS Collaboration

Abstract

The cross sections for charged and neutral current deep inelastic scattering in e^+p collisions with a longitudinally polarised positron beam have been measured using the ZEUS detector at HERA. The results, based on data corresponding to an integrated luminosity of 23.8 pb^{-1} at $\sqrt{s} = 318 \text{ GeV}$, are given for both e^+p charged current and neutral current deep inelastic scattering for both positive and negative values of the longitudinal polarisation of the positron beam. Single differential cross sections are presented for the kinematic region $Q^2 > 200 \text{ GeV}^2$. The measured cross sections are compared to the predictions of the Standard Model. A fit to the data yields $\sigma^{\text{CC}}(P_e = -1) = 7.4 \pm 3.9(\text{stat.}) \pm 1.2(\text{syst.}) \text{ pb}$, which is consistent within two standard deviations with the absence of right-handed charged currents in the Standard Model.

Dedicated to our friend and colleague Nikolaj Pavel.

The ZEUS Collaboration

S. Chekanov, M. Derrick, S. Magill, S. Miglioranza¹, B. Musgrave, D. Nicholass¹, J. Repond, R. Yoshida

Argonne National Laboratory, Argonne, Illinois 60439-4815, USA ⁿ

M.C.K. Mattingly

Andrews University, Berrien Springs, Michigan 49104-0380, USA

N. Pavel, A.G. Yagües Molina

Institut für Physik der Humboldt-Universität zu Berlin, Berlin, Germany

S. Antonelli, P. Antonioli, G. Bari, M. Basile, L. Bellagamba, M. Bindi, D. Boscherini, A. Bruni, G. Bruni, L. Cifarelli, F. Cindolo, A. Contin, M. Corradi, S. De Pasquale, G. Iacobucci, A. Margotti, R. Nania, A. Polini, L. Rinaldi, G. Sartorelli, A. Zichichi

University and INFN Bologna, Bologna, Italy ^e

G. Aghuzumtsyan, D. Bartsch, I. Brock, S. Goers, H. Hartmann, E. Hilger, H.-P. Jakob, M. Jüngst, O.M. Kind, E. Paul², J. Rautenberg, R. Renner, U. Samson³, V. Schönberg, M. Wang, M. Wlasenko

Physikalisches Institut der Universität Bonn, Bonn, Germany ^b

N.H. Brook, G.P. Heath, J.D. Morris, T. Namsou

H.H. Wills Physics Laboratory, University of Bristol, Bristol, United Kingdom ^m

M. Capua, S. Fazio, A. Mastroberardino, M. Schioppa, G. Susinno, E. Tassi

Calabria University, Physics Department and INFN, Cosenza, Italy ^e

J.Y. Kim⁴, K.J. Ma⁵

Chonnam National University, Kwangju, South Korea ^g

Z.A. Ibrahim, B. Kamaluddin, W.A.T. Wan Abdullah

Jabatan Fizik, Universiti Malaya, 50603 Kuala Lumpur, Malaysia ^r

Y. Ning, Z. Ren, W.B. Schmidke, F. Sciulli

Nevis Laboratories, Columbia University, Irvington on Hudson, New York 10027 ^o

J. Chwastowski, A. Eskreys, J. Figiel, A. Galas, M. Gil, K. Olkiewicz, P. Stopa, L. Zawiejski

The Henryk Niewodniczanski Institute of Nuclear Physics, Polish Academy of Sciences, Cracow, Poland ⁱ

L. Adamczyk, T. Bołd, I. Grabowska-Bołd, D. Kisielewska, J. Łukasik, M. Przybycień, L. Suszycki, *Faculty of Physics and Applied Computer Science, AGH-University of Science and Technology, Cracow, Poland ^p*

A. Kotański⁶, W. Słomiński

Department of Physics, Jagellonian University, Cracow, Poland

V. Adler, U. Behrens, I. Bloch, A. Bonato, K. Borrás, N. Coppola, J. Fourletova, A. Geiser, D. Gladkov, P. Göttlicher⁷, I. Gregor, O. Gutsche, T. Haas, W. Hain, C. Horn, B. Kahle, U. Kötz, H. Kowalski, H. Lim⁸, E. Lobodzinska, B. Löhr, R. Mankel, I.-A. Melzer-Pellmann, A. Montanari, C.N. Nguyen, D. Notz, A.E. Nuncio-Quiroz, R. Santamarta, U. Schneekloth, H. Stadie, U. Stösslein, D. Szuba, J. Szuba⁹ T. Theedt, G. Watt, G. Wolf, K. Wrona, C. Youngman, W. Zeuner

Deutsches Elektronen-Synchrotron DESY, Hamburg, Germany

S. Schlenstedt

Deutsches Elektronen-Synchrotron DESY, Zeuthen, Germany

G. Barbagli, E. Gallo, P. G. Pelfer

University and INFN, Florence, Italy^e

A. Bamberger, A. Benen, D. Dobur, F. Karstens, N.N. Vlasov¹⁰

Fakultät für Physik der Universität Freiburg i.Br., Freiburg i.Br., Germany^b

P.J. Bussey, A.T. Doyle, W. Dunne, J. Ferrando, D.H. Saxon, I.O. Skillicorn

Department of Physics and Astronomy, University of Glasgow, Glasgow, United Kingdom^m

I. Gialas¹¹

Department of Engineering in Management and Finance, Univ. of Aegean, Greece

T. Gosau, U. Holm, R. Klanner, E. Lohrmann, H. Salehi, P. Schleper, T. Schörner-Sadenius, J. Sztuk, K. Wichmann, K. Wick

Hamburg University, Institute of Exp. Physics, Hamburg, Germany^b

C. Foudas, C. Fry, K.R. Long, A.D. Tapper

Imperial College London, High Energy Nuclear Physics Group, London, United Kingdom^m

M. Kataoka¹², K. Nagano, K. Tokushuku¹³, S. Yamada, Y. Yamazaki

Institute of Particle and Nuclear Studies, KEK, Tsukuba, Japan^f

A.N. Barakbaev, E.G. Boos, A. Dossanov, N.S. Pokrovskiy, B.O. Zhautykov

Institute of Physics and Technology of Ministry of Education and Science of Kazakhstan, Almaty, Kazakhstan

D. Son

Kyungpook National University, Center for High Energy Physics, Daegu, South Korea^g

J. de Favereau, K. Piotrkowski

Institut de Physique Nucléaire, Université Catholique de Louvain, Louvain-la-Neuve, Belgium^g

F. Barreiro, C. Glasman¹⁴, M. Jimenez, L. Labarga, J. del Peso, E. Ron, J. Terrón, M. Zambrana

Departamento de Física Teórica, Universidad Autónoma de Madrid, Madrid, Spain^l

F. Corriveau, C. Liu, R. Walsh, C. Zhou

Department of Physics, McGill University, Montréal, Québec, Canada H3A 2T8^a

T. Tsurugai

Meiji Gakuin University, Faculty of General Education, Yokohama, Japan^f

A. Antonov, B.A. Dolgoshein, I. Rubinsky, V. Sosnovtsev, A. Stifutkin, S. Suchkov

Moscow Engineering Physics Institute, Moscow, Russia^j

R.K. Dementiev, P.F. Ermolov, L.K. Gladilin, I.I. Katkov, L.A. Khein, I.A. Korzhavina, V.A. Kuzmin, B.B. Levchenko, O.Yu. Lukina, A.S. Proskuryakov, L.M. Shcheglova, D.S. Zotkin, S.A. Zotkin

Moscow State University, Institute of Nuclear Physics, Moscow, Russia^k

I. Abt, C. Büttner, A. Caldwell, D. Kollar, X. Liu, J. Sutiak

Max-Planck-Institut für Physik, München, Germany

G. Grigorescu, A. Keramidas, E. Koffeman, P. Kooijman, E. Maddox, H. Tiecke, M. Vázquez¹⁵, L. Wiggers

NIKHEF and University of Amsterdam, Amsterdam, Netherlands^h

N. Brümmer, B. Bylsma, L.S. Durkin, A. Lee, T.Y. Ling

Physics Department, Ohio State University, Columbus, Ohio 43210ⁿ

P.D. Allfrey, M.A. Bell, A.M. Cooper-Sarkar, A. Cottrell, R.C.E. Devenish, B. Foster, C. Gwenlan¹⁶, K. Korcsak-Gorzo, S. Patel, V. Roberfroid¹⁷, A. Robertson, P.B. Straub, C. Uribe-Estrada, R. Walczak

Department of Physics, University of Oxford, Oxford United Kingdom^m

P. Bellan, A. Bertolin, R. Brugnera, R. Carlin, R. Ciesielski, F. Dal Corso, S. Dusini, A. Garfagnini, S. Limentani, A. Longhin, L. Stanco, M. Turcato

Dipartimento di Fisica dell' Università and INFN, Padova, Italy^e

B.Y. Oh, A. Raval, J.J. Whitmore

Department of Physics, Pennsylvania State University, University Park, Pennsylvania 16802^o

Y. Iga

Polytechnic University, Sagamihara, Japan^f

G. D'Agostini, G. Marini, A. Nigro
Dipartimento di Fisica, Università 'La Sapienza' and INFN, Rome, Italy^e

J.E. Cole, J.C. Hart
Rutherford Appleton Laboratory, Chilton, Didcot, Oxon, United Kingdom^m

H. Abramowicz¹⁸, A. Gabareen, S. Kananov, A. Levy
Raymond and Beverly Sackler Faculty of Exact Sciences, School of Physics, Tel-Aviv University, Tel-Aviv, Israel^d

M. Kuze
Department of Physics, Tokyo Institute of Technology, Tokyo, Japan^f

R. Hori, S. Kagawa¹⁹, S. Shimizu, T. Tawara
Department of Physics, University of Tokyo, Tokyo, Japan^f

R. Hamatsu, H. Kaji, S. Kitamura²⁰, O. Ota, Y.D. Ri
Tokyo Metropolitan University, Department of Physics, Tokyo, Japan^f

M.I. Ferrero, V. Monaco, R. Sacchi, A. Solano, A. Staiano
Università di Torino and INFN, Torino, Italy^e

M. Arneodo, M. Ruspa
Università del Piemonte Orientale, Novara, and INFN, Torino, Italy^e

S. Fourletov, J.F. Martin
Department of Physics, University of Toronto, Toronto, Ontario, Canada M5S 1A7^a

J.M. Butterworth, R. Hall-Wilton¹⁵, T.W. Jones, J.H. Loizides, M.R. Sutton²¹, C. Targett-Adams, M. Wing
Physics and Astronomy Department, University College London, London, United Kingdom^m

B. Brzozowska, J. Ciborowski²², G. Grzelak, P. Kulinski, P. Łuźniak²³, J. Malka²³, R.J. Nowak, J.M. Pawlak, T. Tymieniecka, A. Ukleja²⁴, J. Ukleja²⁵, A.F. Żarnecki
Warsaw University, Institute of Experimental Physics, Warsaw, Poland

M. Adamus, P. Plucinski²⁶
Institute for Nuclear Studies, Warsaw, Poland

Y. Eisenberg, D. Hochman, U. Karshon
Department of Particle Physics, Weizmann Institute, Rehovot, Israel^c

E. Brownson, T. Danielson, A. Everett, D. Kçira, D.D. Reeder, M. Rosin, P. Ryan, A.A. Savin, W.H. Smith, H. Wolfe
*Department of Physics, University of Wisconsin, Madison, Wisconsin 53706, USA*ⁿ

S. Bhadra, C.D. Catterall, Y. Cui, G. Hartner, S. Menary, U. Noor, M. Soares, J. Standage,
J. Whyte

Department of Physics, York University, Ontario, Canada M3J 1P3^a

- ¹ also affiliated with University College London, UK
- ² retired
- ³ formerly U. Meyer
- ⁴ supported by Chonnam National University in 2005
- ⁵ supported by a scholarship of the World Laboratory Björn Wiik Research Project
- ⁶ supported by the research grant no. 1 P03B 04529 (2005-2008)
- ⁷ now at DESY group FEB, Hamburg, Germany
- ⁸ now at Argonne National Laboratory, Argonne, IL, USA
- ⁹ on leave of absence from FPACS, AGH-UST, Cracow, Poland
- ¹⁰ partly supported by Moscow State University, Russia
- ¹¹ also affiliated with DESY
- ¹² now at ICEPP, University of Tokyo, Japan
- ¹³ also at University of Tokyo, Japan
- ¹⁴ Ramón y Cajal Fellow
- ¹⁵ now at CERN, Geneva, Switzerland
- ¹⁶ PPARC Postdoctoral Research Fellow
- ¹⁷ EU Marie Curie Fellow
- ¹⁸ also at Max Planck Institute, Munich, Germany, Alexander von Humboldt Research Award
- ¹⁹ now at KEK, Tsukuba, Japan
- ²⁰ Department of Radiological Science
- ²¹ PPARC Advanced fellow
- ²² also at Łódź University, Poland
- ²³ Łódź University, Poland
- ²⁴ supported by the Polish Ministry for Education and Science grant no. 1 P03B 12629
- ²⁵ supported by the KBN grant no. 2 P03B 12725
- ²⁶ supported by the Polish Ministry for Education and Science grant no. 1 P03B 14129

- ^a supported by the Natural Sciences and Engineering Research Council of Canada (NSERC)
- ^b supported by the German Federal Ministry for Education and Research (BMBF), under contract numbers HZ1GUA 2, HZ1GUB 0, HZ1PDA 5, HZ1VFA 5
- ^c supported in part by the MINERVA Gesellschaft für Forschung GmbH, the Israel Science Foundation (grant no. 293/02-11.2) and the U.S.-Israel Binational Science Foundation
- ^d supported by the German-Israeli Foundation and the Israel Science Foundation
- ^e supported by the Italian National Institute for Nuclear Physics (INFN)
- ^f supported by the Japanese Ministry of Education, Culture, Sports, Science and Technology (MEXT) and its grants for Scientific Research
- ^g supported by the Korean Ministry of Education and Korea Science and Engineering Foundation
- ^h supported by the Netherlands Foundation for Research on Matter (FOM)
- ⁱ supported by the Polish State Committee for Scientific Research, grant no. 620/E-77/SPB/DESY/P-03/DZ 117/2003-2005 and grant no. 1P03B07427/2004-2006
- ^j partially supported by the German Federal Ministry for Education and Research (BMBF)
- ^k supported by RF Presidential grant N 1685.2003.2 for the leading scientific schools and by the Russian Ministry of Education and Science through its grant for Scientific Research on High Energy Physics
- ^l supported by the Spanish Ministry of Education and Science through funds provided by CICYT
- ^m supported by the Particle Physics and Astronomy Research Council, UK
- ⁿ supported by the US Department of Energy
- ^o supported by the US National Science Foundation
- ^p supported by the Polish Ministry of Scientific Research and Information Technology, grant no. 112/E-356/SPUB/DESY/P-03/DZ 116/2003-2005 and 1 P03B 065 27
- ^q supported by FNRS and its associated funds (IISN and FRiA) and by an Inter-University Attraction Poles Programme subsidised by the Belgian Federal Science Policy Office
- ^r supported by the Malaysian Ministry of Science, Technology and Innovation/Akademi Sains Malaysia grant SAGA 66-02-03-0048

1 Introduction

Deep inelastic scattering (DIS) of leptons off nucleons is an important process in the understanding of the structure of the proton and has been vital in the development of the Standard Model (SM). The HERA ep collider allows the exploration of DIS at high values of the negative four-momentum-transfer squared, Q^2 . Using data taken in the years 1994–2000 the H1 and ZEUS collaborations have reported measurements of the cross sections for charged current (CC) and neutral current (NC) DIS [1–10]. These measurements extend the kinematic region covered by fixed-target experiments [11] to higher Q^2 values and probe the electroweak sector of the Standard Model.

Polarised electron-nucleon deep inelastic scattering was first performed in the 1970s at low values of Q^2 . The results established parity violation attributable to the weak neutral current [12]. Since 2002, the upgraded HERA collider has delivered longitudinally polarised lepton beams to the collider experiments. The luminosity was also higher than in previous years. In the kinematic range of HERA, the SM predicts that the cross sections for charged and neutral current ep DIS should exhibit specific dependencies on the longitudinal polarisation of the incoming lepton beam. The absence of right-handed charged currents leads to the prediction that the charged current cross section will be a linear function of polarisation, vanishing for right-handed (left-handed) electron (positron) beams.

This paper presents measurements of the cross sections for e^+p CC and NC DIS at high Q^2 with longitudinally polarised positron beams using the ZEUS detector. The measurements are based on 11.5 pb^{-1} of data collected between April and June 2004 at a mean luminosity-weighted polarisation of -0.41 , and 12.3 pb^{-1} collected between June and August 2004 at a polarisation of $+0.32$. During this time HERA collided protons of energy 920 GeV with positrons of energy 27.5 GeV, yielding collisions at a centre-of-mass energy of 318 GeV. The measured cross sections are compared to the predictions of the SM. Similar results have recently been published by the H1 Collaboration [13].

2 Standard Model predictions

Inclusive deep inelastic lepton-proton scattering can be described in terms of the kinematic variables x and Q^2 . The variable Q^2 is defined by $Q^2 = -q^2 = -(k - k')^2$ where k and k' are the four-momenta of the incoming and scattered lepton, respectively. Bjorken x is defined by $x = Q^2/(2P \cdot q)$, where P is the four-momentum of the incoming proton. The inelasticity variable y is determined from $Q^2 = sxy$, where $s = 4E_e E_p$ is the square of the lepton-proton centre-of-mass energy (neglecting the masses of the incoming particles).

The electroweak Born level cross section for the CC reaction

$$e^+p \rightarrow \bar{\nu}_e X,$$

with a longitudinally polarised positron beam, can be expressed at leading order in QCD as [14]

$$\frac{d^2\sigma^{\text{CC}}(e^+p)}{dx dQ^2} = (1 + P_e) \frac{G_F^2}{4\pi x} \left(\frac{M_W^2}{M_W^2 + Q^2} \right)^2 \cdot \left[Y_+ F_2^{\text{CC}}(x, Q^2) - Y_- x F_3^{\text{CC}}(x, Q^2) \right],$$

where G_F is the Fermi constant, M_W is the mass of the W boson and $Y_{\pm} = 1 \pm (1 - y)^2$. The structure-functions F_2^{CC} and $x F_3^{\text{CC}}$ may be written in terms of sums and differences of quark and antiquark parton density functions (PDFs) of the proton as follows:

$$F_2^{\text{CC}} = x[d(x, Q^2) + s(x, Q^2) + \bar{u}(x, Q^2) + \bar{c}(x, Q^2)],$$

$$x F_3^{\text{CC}} = x[d(x, Q^2) + s(x, Q^2) - \bar{u}(x, Q^2) - \bar{c}(x, Q^2)],$$

where, for example, the PDF $d(x, Q^2)$ gives the number density of down quarks with momentum-fraction x at a given Q^2 . The longitudinal polarisation of the positron beam is defined as

$$P_e = \frac{N_R - N_L}{N_R + N_L},$$

where N_R and N_L are the numbers of right¹- and left-handed positrons in the beam, respectively. Similarly the cross section for the NC reaction

$$e^+p \rightarrow e^+ X,$$

can be expressed as [14]

$$\frac{d^2\sigma^{\text{NC}}(e^+p)}{dx dQ^2} = \frac{2\pi\alpha^2}{xQ^4} [H_0^+ - P_e H_{P_e}^+],$$

¹ At HERA beam energies the mass of the incoming leptons may be neglected, and therefore the difference between handedness and helicity may also be neglected.

where α is the QED coupling constant and H_0^+ and $H_{P_e}^+$ contain the unpolarised and polarised structure functions, respectively, such that at leading order in QCD

$$H_0^+ = Y_+ F_2^0 - Y_- x F_3^0, \quad F_2^0 = \sum_q x(q + \bar{q}) A_q^0, \quad x F_3^0 = \sum_q x(q - \bar{q}) B_q^0,$$

and

$$H_{P_e}^+ = Y_+ F_2^{P_e} - Y_- x F_3^{P_e}, \quad F_2^{P_e} = \sum_q x(q + \bar{q}) A_q^{P_e}, \quad x F_3^{P_e} = \sum_q x(q - \bar{q}) B_q^{P_e},$$

where q and \bar{q} are the quark and antiquark PDFs, respectively, and the sums run over the five active quark flavours. The A and B coefficients contain the quark and positron couplings to the photon and Z boson and are given by

$$A_q^0 = e_q^2 - 2e_q v_q v_e \chi_Z + (v_q^2 + a_q^2)(v_e^2 + a_e^2) \chi_Z^2,$$

$$B_q^0 = -2e_q a_q a_e \chi_Z + 4v_q a_q v_e a_e \chi_Z^2,$$

and

$$A_q^{P_e} = 2e_q v_q a_e \chi_Z - 2(v_q^2 + a_q^2) v_e a_e \chi_Z^2,$$

$$B_q^{P_e} = 2e_q a_q v_e \chi_Z - 2v_q a_q (v_e^2 + a_e^2) \chi_Z^2,$$

where e_f is the electric charge in units of the positron charge and a_f and v_f are the axial and vector couplings of the fermion f . The couplings are defined by $a_f = I_3^f$ and $v_f = I_3^f - 2e_f \sin^2 \theta_W$ where I_3^f is the third component of weak isospin and θ_W is the Weinberg angle. The quantity χ_Z is proportional to the ratio of the Z^0 and photon propagators:

$$\chi_Z = \frac{1}{\sin^2 2\theta_W} \left(\frac{Q^2}{M_Z^2 + Q^2} \right),$$

where M_Z is the mass of the Z^0 boson.

3 Experimental apparatus

A detailed description of the ZEUS detector can be found elsewhere [15]. A brief outline of the components most relevant for this analysis is given below.

Charged particles are tracked in the central tracking detector (CTD) [16], which operates in a magnetic field of 1.43 T provided by a thin superconducting solenoid. The CTD consists of 72 cylindrical drift chamber layers, organised in nine superlayers covering the polar-angle² region $15^\circ < \theta < 164^\circ$. In 2001 a silicon microvertex detector (MVD) [17] was installed between the beampipe and the inner radius of the CTD. The MVD is organised into a barrel with 3 cylindrical layers and a forward section with four planar layers perpendicular to the HERA beam direction. The barrel contains 600 single-sided silicon strip sensors each having 512 strips of width $120\ \mu\text{m}$; the forward section contains 112 sensors each of which has 480 strips of width $120\ \mu\text{m}$. Charged-particle tracks were reconstructed using information from the CTD and MVD.

The high-resolution uranium–scintillator calorimeter (CAL) [18] consists of three parts: the forward (FCAL), the barrel (BCAL) and the rear (RCAL) calorimeter, covering 99.7% of the solid angle around the nominal interaction point. Each part is subdivided transversely into towers and longitudinally into one electromagnetic section (EMC) and either one (in RCAL) or two (in BCAL and FCAL) hadronic sections (HAC). The smallest subdivision of the calorimeter is called a cell. The CAL relative energy resolutions, as measured under test-beam conditions, are $\sigma(E)/E = 0.18/\sqrt{E}$ for electrons and $\sigma(E)/E = 0.35/\sqrt{E}$ for hadrons, with E in GeV. The timing resolution of the CAL is better than 1 ns for energy deposits exceeding 4.5 GeV. The position of the interaction vertex along the beam direction can be reconstructed from the arrival time of energy deposits in FCAL. The resolution is about 10 cm for events with FCAL energy above 25 GeV, improving to about 8 cm for FCAL energy above 100 GeV.

An iron structure that surrounds the CAL is instrumented as a backing calorimeter (BAC) [19] to measure energy leakage from the CAL. Muon chambers in the forward, barrel and rear [20] regions are used in this analysis to veto background events induced by cosmic-ray or beam-halo muons.

The luminosity was measured using the Bethe-Heitler reaction $ep \rightarrow e\gamma p$ by the luminosity detector which consists of two independent systems. In the first system the photons are detected by a lead–scintillator calorimeter placed in the HERA tunnel 107 m from the

² The ZEUS coordinate system is a right-handed Cartesian system, with the Z axis pointing in the proton beam direction, referred to as the “forward direction”, and the X axis pointing left towards the centre of HERA. The polar angle, θ , is measured with respect to the proton beam direction. The coordinate origin is at the nominal interaction point.

interaction point in the positron-beam direction. The system used in previous ZEUS publications [21] was modified by the addition of active filters in order to suppress the increased synchrotron radiation background of the upgraded HERA collider. The second system is a magnetic spectrometer arrangement [22]. A small fraction ($\sim 9\%$) of the small-angle energetic photons from the Bethe-Heitler process convert in the exit window of the vacuum chamber. Electron-positron pairs from the converted photons were bent vertically by a dipole magnet and detected in tungsten-scintillator calorimeters located above and below the photon beam at $Z = -104$ m. The advantage of the spectrometer system is that it does not suffer from pile-up (multiple interactions at high luminosity) and is not sensitive to direct synchrotron radiation, whereas the calorimeter system has higher acceptance. The fractional uncertainty on the measured luminosity was 3.5%.

The lepton beam in HERA becomes naturally transversely polarised through the Sokolov-Ternov effect [23]. The characteristic build-up time expected for the HERA accelerator is approximately 40 minutes. Spin rotators on either side of the ZEUS detector change the transverse polarisation of the beam into longitudinal polarisation. The positron beam polarisation was measured using two independent polarimeters, the transverse polarimeter (TPOL) [24] and the longitudinal polarimeter (LPOL) [25]. Both devices exploit the spin-dependent cross section for Compton scattering of circularly polarised photons off positrons to measure the beam polarisation. The transverse polarimeter was upgraded in 2001 to provide a fast measurement for every positron bunch, and position-sensitive silicon strip and scintillating-fibre detectors were added to investigate systematic effects [26]. The luminosity and polarisation measurements were made over times that were much shorter than the polarisation build-up time.

4 Monte Carlo simulation

Monte Carlo (MC) simulations were used to determine the efficiency for selecting events and the accuracy of kinematic reconstruction, to estimate the ep background rate and to extrapolate the measured cross sections to the full kinematic region. A sufficient number of events were generated to ensure that uncertainties from MC statistics were small compared to other uncertainties.

Neutral and charged current DIS events including radiative effects were simulated using the DJANGO [27] generator. The polarisation dependence of radiative effects in CC DIS, neglected in DJANGO, was checked using the GRACE [28] program and found to be negligible. The hadronic final state was simulated using the colour-dipole model of ARIADNE 4.10 [29] and, as a systematic check, the MEPS model of LEPTO 6.5 [30]. Both programs use the Lund string model of JETSET 7.4 [31] for the hadronisation. The

photoproduction background was estimated using events simulated with HERWIG 5.9 [32]. Diffractive NC events were generated using the RAPGAP 2.08/06 [33] program and mixed with the non-diffractive MC events in order to simulate the hadronic final state accurately. Background to the CC signal from W production was estimated using the EPVEC 1.0 [34] generator and background from the production of charged-lepton pairs was generated using the GRAPE 1.1 [35] program.

5 Kinematic Reconstruction

Charged current events are characterised by a large missing transverse momentum, $P_{T,\text{miss}}$, the magnitude of which is calculated as

$$P_{T,\text{miss}}^2 = P_x^2 + P_y^2 = \left(\sum_i E_i \sin \theta_i \cos \phi_i \right)^2 + \left(\sum_i E_i \sin \theta_i \sin \phi_i \right)^2,$$

where the sum runs over all calorimeter energy deposits E_i , (corrected [4] for energy loss in inactive material and other effects in the offline analysis) and θ_i and ϕ_i are the polar and azimuthal angles of the calorimeter energy deposit as viewed from the interaction vertex. The hadronic polar angle, γ_h , is defined by $\cos \gamma_h = (P_{T,\text{miss}}^2 - \delta^2)/(P_{T,\text{miss}}^2 + \delta^2)$, where $\delta = \sum (E_i - E_i \cos \theta_i) = \sum (E - P_z)_i$. In the naive Quark Parton Model, γ_h gives the scattering angle of the struck quark in the lab frame. The total transverse energy, E_T , is given by $E_T = \sum E_i \sin \theta_i$. The kinematic variables x_{JB} , y_{JB} and Q_{JB}^2 for charged current events were reconstructed from the measured $P_{T,\text{miss}}$ and δ using the Jacquet-Blondel method [36].

Neutral current events are characterised by the presence of a high-energy isolated scattered positron in the detector. It follows from longitudinal momentum conservation that for well measured NC events, δ peaks at twice the positron beam energy or 55 GeV. The hadronic transverse momentum, $P_{T,h}$, and δ_h were calculated in the same way as the corresponding quantities in CC events, but excluding energy deposits associated with the scattered positron. The hadronic polar angle, γ_h , was calculated from $P_{T,h}$ and δ_h in the same way as the CC case. The scattered positron energy, E'_e , and polar angle, θ_e , were determined from the energy deposit and matched track of the scattered positron candidate, respectively.

The double-angle method [37] was used to estimate the kinematic variables x_{DA} , y_{DA} and Q_{DA}^2 for the neutral current events using the measured values of θ_e and γ_h .

6 Event selection

6.1 Charged current

The following criteria were imposed to select CC events and to reject background:

- missing transverse momentum: $P_{T,\text{miss}} > 12 \text{ GeV}$ was required and, in addition, the missing transverse momentum, excluding the calorimeter cells adjacent to the forward beam hole, $P'_{T,\text{miss}}$, was required to satisfy $P'_{T,\text{miss}} > 10 \text{ GeV}$;
- primary vertex: events were required to satisfy $|Z_{\text{VTX}}| < 50 \text{ cm}$. The Z coordinate of the vertex, reconstructed using the tracking detectors, was required to be consistent with that of an ep interaction. For events with an hadronic angle, γ_h , of less than 23° , the vertex Z position was reconstructed from the measured arrival time of energy deposits in FCAL [38], and the $P_{T,\text{miss}}$ and $P'_{T,\text{miss}}$ thresholds were increased to 14 and 12 GeV, respectively;
- rejection of photoproduction: $P_{T,\text{miss}}/E_T > 0.4$ was required for events with $20 < P_{T,\text{miss}} < 30 \text{ GeV}$; $P_{T,\text{miss}}/E_T > 0.55$ was required for events with $P_{T,\text{miss}} < 20 \text{ GeV}$. These requirements select events with an azimuthally collimated energy flow. In addition, it was required that the angle between the transverse momentum measured using the tracks and that measured by the calorimeter was less than one radian for events with $P_{T,\text{miss}} < 30 \text{ GeV}$;
- rejection of NC DIS: NC DIS events in which the scattered positron or the hadronic system is poorly measured can have significant missing transverse momentum. Events with $\delta > 30 \text{ GeV}$ and an isolated electromagnetic cluster with energy of at least 4 GeV measured in the calorimeter were rejected;
- rejection of non- ep background: interactions between one of the beams and the residual gas in the beam pipe or upstream accelerator components can lead to events with significant missing transverse momentum. However, for such interactions, the arrival times of energy deposits in the calorimeter are inconsistent with the bunch-crossing time and were used to reject such events. Muon-finding algorithms based on tracking, calorimeter and muon-chamber information were used to reject events caused by cosmic rays or muons in the beam halo. In addition, the shape of hadronic showers in the calorimeter was used to reject halo-muon events depositing energy in the forward calorimeter. Further details can be found elsewhere [39, 40];
- kinematic region: events were required to satisfy $Q_{\text{JB}}^2 > 200 \text{ GeV}^2$ and $y_{\text{JB}} < 0.9$. These requirements restricted the event sample to a region where the resolution of the kinematic quantities was good and the background was small [9].

All events were visually inspected; 12 cosmic-ray and halo-muon events were removed from the negative-polarisation sample and 8 from the positive-polarisation sample. A total of 158 data events satisfied all criteria in the negative-polarisation sample and 311 in the positive-polarisation sample.

The main background remaining after the selection was photoproduction events, the cross section for which is independent of the longitudinal polarisation of the positron beam. The contamination was estimated from MC to be typically less than 1% but was as high as 5% in the lowest- Q^2 bin of the negative-polarisation sample.

Figure 1 shows a comparison of data and MC distributions for the CC sample. The MC sample, which was weighted to the measured polarisations and luminosities of the data samples, gives a satisfactory description of the data.

6.2 Neutral current

The following criteria were imposed to select NC events:

- positron identification: an algorithm which combined information from the energy deposits in the calorimeter with tracks was used to identify scattered positrons. A fiducial-volume cut was applied to guarantee that the experimental acceptance was well understood [10]. To ensure high purity and reject background, the identified positron was required to have an energy of at least 10 GeV and be isolated such that the energy in an $\eta - \phi$ cone of radius 0.8 centred on the positron, but not associated with it, was less than 5 GeV. For events in which a positron was found within the acceptance of the tracking detectors, a track matched to the energy deposit in the calorimeter was required. For events with a positron at a smaller polar angle than the acceptance of the tracking detectors, the track requirement was replaced with the requirement that the transverse momentum of the positron exceed 30 GeV;
- primary vertex: events were required to satisfy $|Z_{\text{VTX}}| < 50$ cm. The Z coordinate of the ep interaction vertex was reconstructed using tracks;
- background rejection: the requirement $38 < \delta < 65$ GeV was imposed to remove photoproduction and beam-gas events, and to reduce the number of events with significant QED initial-state radiation. The lower threshold was increased to 44 GeV for events which did not have a track matched to the positron candidate. To further reduce background from photoproduction, y calculated using the electron method was required to satisfy $y_e < 0.95$. The net transverse momentum is expected to be small, so, in order to remove cosmic-ray events and beam related background events, the quantity $P_{T,\text{miss}}/\sqrt{E_T}$ was required to be less than $4\sqrt{\text{GeV}}$, and the quantity $P_{T,\text{miss}}/E_T$ was required to be less than 0.7;

- QED Compton rejection: to reduce the size of the QED radiative corrections, elastic Compton-scattering events were rejected. The contribution from deeply-virtual Compton scattering was negligible;
- kinematic region: to avoid regions of phase space in which the MC generator was not valid, the quantity $y_{\text{JB}}(1 - x_{\text{DA}})$ was required to be greater than 0.004. The final event sample was defined by requiring $Q_{\text{DA}}^2 > 200 \text{ GeV}^2$.

A total of 20642 events passed the selection criteria in the negative polarisation sample and 22395 in the positive polarisation sample. The background contamination, dominated by misidentified photoproduction, was typically less than 1%. Figure 2 shows a comparison of data and MC distributions for the NC sample. The MC sample gives a generally good description of the data. The effect of the positron fiducial-volume cuts can be seen in the positron angle ($\sim 2.4 \text{ rad}$) and Q^2 ($\sim 600 \text{ GeV}^2$) distributions.

7 Cross section determination

The measured cross section in a particular kinematic bin, for example in $d\sigma/dQ^2$, was determined from

$$\frac{d\sigma_{\text{Born}}}{dQ^2} = \frac{N_{\text{data}} - N_{\text{bg}}}{N_{\text{MC}}} \cdot \frac{d\sigma_{\text{Born}}^{\text{SM}}}{dQ^2},$$

where N_{data} is the number of data events, N_{bg} is the number of background events estimated from the MC simulation and N_{MC} is the number of signal MC events. The SM prediction $d\sigma_{\text{Born}}^{\text{SM}}/dQ^2$ was evaluated in the on-shell scheme using the PDG [41] values for the electroweak parameters and the CTEQ5D PDFs [42]. A similar procedure was used for $d\sigma/dx$ and $d\sigma/dy$.

The major sources of systematic uncertainty in the CC cross sections come from the uncertainties in calorimeter energy scale and the parton-shower scheme. The former was estimated using a method detailed in previous publications [7,9] for the NC data sample. The resulting shifts in the cross sections were typically less than 10%, but increased to 20% in the highest Q^2 bin and 30% in the highest x bin.

To estimate the sensitivity of the results to the details of the simulation of the hadronic final state, the LEPTO MEPS model was used instead of the ARIADNE model for calculating the acceptance corrections. The largest effects of $\sim 5\%$ were observed in the highest Q^2 and x bins.

The uncertainty in the small contribution from photoproduction was estimated by fitting a linear combination of the $P_{T,\text{miss}}/E_T$ distributions of the signal and the background MC samples to the corresponding distribution in the data, allowing the normalisation of the photoproduction MC events to vary. No cut on $P_{T,\text{miss}}/E_T$ was applied for this check. Varying the normalisation of the photoproduction events by the uncertainty in the fit of $\pm 30\%$ resulted in changes of the measured cross sections within $\pm 3\%$.

The systematic uncertainties of the selection cuts were estimated by varying the threshold value of each selection cut independently by around 10%, which is a reasonable match to the resolution. The resulting shifts in the cross sections were typically within $\pm 5\%$.

A major source of systematic uncertainty in the NC cross section came from the uncertainty in the parton-shower scheme, which gave changes in the cross section of typically within $\pm 2\%$ but up to 4% at high Q^2 . Uncertainty in the electromagnetic energy scale was estimated by varying the energy scale by $\pm 1\%$. However, due to the use of the double-angle reconstruction, the resulting shifts in the cross section were typically $< 0.5\%$. The systematic effects of the selection cuts were estimated by varying the threshold value of each selection cut independently by values commensurate with the resolutions. The resulting shifts in the cross sections were typically within $\pm 1\%$.

The individual uncertainties were added in quadrature separately for the positive and negative deviations from the nominal cross-section values to obtain the total systematic uncertainty. The uncertainty in the measured polarisation, $\delta P_e/P_e$, was 1.6% using the LPOL and 3.5% using the TPOL. The choice of polarimeter measurement was made to maximise the available luminosity for the analysis, while minimising the uncertainty in the measured polarisation, on a run-by-run basis.

The relative uncertainty in the measured luminosity of 3.5% was not included in the total uncertainty shown in the differential cross-section figures.

8 Results

In the following, measurements of total cross sections and differential cross sections in x , y and Q^2 for the charged current reaction are presented. In addition, cross sections differential in Q^2 were measured for the neutral current reaction.

The total cross sections for e^+p CC DIS in the kinematic region $Q^2 > 200 \text{ GeV}^2$ are

$$\sigma^{\text{CC}}(P_e = 0.32 \pm 0.01) = 42.8 \pm 2.4(\text{stat.}) \pm 1.9(\text{syst.}) \text{ pb},$$

and

$$\sigma^{\text{CC}}(P_e = -0.41 \pm 0.01) = 23.3 \pm 1.9(\text{stat.}) \pm 1.0(\text{syst.}) \text{ pb.}$$

including the uncertainty from the measured luminosity. The total cross section is shown as a function of the longitudinal polarisation of the positron beam in Fig. 3, including the unpolarised ZEUS measurement from the 1999-2000 data [9]. The data are compared to the Standard Model prediction evaluated using the ZEUS-JETS [43] and CTEQ6D [44] PDFs. The SM prediction describes the data well. A linear fit to the data yields an extrapolated value of

$$\sigma^{\text{CC}}(P_e = -1) = 7.4 \pm 3.9(\text{stat.}) \pm 1.2(\text{syst.}) \text{ pb,}$$

with $\chi^2 = 0.1$, consistent within two standard deviations with the absence of right-handed charged currents in the SM. In the fit, the systematic uncertainties of the two polarised data points were considered fully correlated and the uncertainties in the measured polarisation fully anti-correlated. The systematic uncertainty in the unpolarised data point was considered to be uncorrelated with the polarised points.

The single-differential cross-sections $d\sigma/dQ^2$, $d\sigma/dx$ and $d\sigma/dy$ for charged current DIS are shown in Fig. 4. A clear difference is observed between the measurements for positive and negative longitudinal polarisation, which is independent of the kinematic variables. The effects are well described by the SM evaluated using the ZEUS-JETS PDFs.

Figure 5 shows the differential cross-section $d\sigma/dQ^2$ for NC DIS for positive and negative longitudinal polarisations and the ratio of the two cross sections. Only statistical uncertainties were considered when taking the ratio of the positively and negatively polarised cross sections. The measurements are well described by the SM evaluated using the ZEUS-JETS PDFs and are consistent with the expectations of the electroweak Standard Model for polarised NC DIS. A χ^2 test for the $Q^2 > 1000 \text{ GeV}^2$ data points yields $\chi^2 = 0.3$ per data point for the SM and 1.5 for no polarisation dependence.

9 Summary

The cross sections for charged and neutral current deep inelastic scattering in e^+p collisions with a longitudinally polarised positron beam have been measured. The measurements are the first from the ZEUS collaboration in the second phase of HERA operation and are based on data corresponding to an integrated luminosity of 23.8 pb^{-1} collected in 2004 at a

centre-of-mass energy of 318 GeV. The cross sections for e^+p charged current deep inelastic scattering are different for positive and negative values of the positron beam longitudinal polarisation. In addition, single differential cross sections are presented for charged and neutral current deep inelastic scattering in the kinematic region $Q^2 > 200 \text{ GeV}^2$. The measured cross sections are well described by the predictions of the Standard Model. A fit to the cross-section measurements yields $\sigma^{\text{CC}}(P_e = -1) = 7.4 \pm 3.9(\text{stat.}) \pm 1.2(\text{syst.}) \text{ pb}$, which is within two standard deviations of the prediction of the Standard Model of zero.

Acknowledgements

We are grateful to the DESY directorate for their strong support and encouragement. We thank the HERA machine group whose outstanding efforts resulted in the successful upgrade of the HERA accelerator which made this work possible. We also thank the HERA polarimeter group for providing the measurements of the lepton-beam polarisation. The design, construction and installation of the ZEUS detector has been made possible by the efforts of many people not listed as authors. It is a pleasure to thank H. Spiesberger and T. Abe for useful discussions.

References

- [1] H1 Collaboration, T. Ahmed et al., Phys. Lett. B 324 (1994) 241;
H1 Collaboration, S. Aid et al., Z. Phys. C 67 (1995) 565;
H1 Collaboration, S. Aid et al., Phys. Lett. B 379 (1996) 319;
H1 Collaboration, S. Aid et al., Nucl. Phys. B 470 (1996) 3;
H1 Collaboration, C. Adloff et al., Nucl. Phys. B 497 (1997) 3;
H1 Collaboration, C. Adloff et al., Eur. Phys. J. C 13 (2000) 609;
H1 Collaboration, C. Adloff et al., Eur. Phys. J. C 19 (2001) 269;
H1 Collaboration, C. Adloff et al., Eur. Phys. J. C 21 (2001) 33;
H1 Collaboration, C. Adloff et al., Eur. Phys. J. C 30 (2003) 1.
- [2] ZEUS Collaboration, M. Derrick et al., Phys. Rev. Lett. 75 (1995) 1006.
- [3] ZEUS Collaboration, M. Derrick et al., Z. Phys. C 72 (1996) 47.
- [4] ZEUS Collaboration, J. Breitweg et al., Eur. Phys. J. C 11 (1999) 427.
- [5] ZEUS Collaboration, J. Breitweg et al., Eur. Phys. J. C 12 (2000) 411. Erratum in Eur. Phys. J. C 27, 305 (2003).
- [6] ZEUS Collaboration, S. Chekanov et al., Eur. Phys. J. C 21 (2001) 443.
- [7] ZEUS Collaboration, S. Chekanov et al., Phys. Lett. B 539 (2002) 197. Erratum in Phys. Lett. B 552, 308 (2003).
- [8] ZEUS Collaboration, S. Chekanov et al., Eur. Phys. J. C 28 (2003) 175.
- [9] ZEUS Collaboration, S. Chekanov et al., Eur. Phys. J. C 32 (2003) 1.
- [10] ZEUS Collaboration, S. Chekanov et al., Phys. Rev. D 70 (2004) 052001.
- [11] CDHS Collaboration, H. Abramowicz et al., Z. Phys. C 25 (1984) 29;
CDHSW Collaboration, J.P. Berge et al., Z. Phys. C 49 (1991) 187;
CCFR Collaboration, E. Oltman et al., Z. Phys. C 53 (1992) 51;
BEBC Collaboration, G.T. Jones et al., Z. Phys. C 62 (1994) 575.
- [12] C.Y. Prescott et al., Phys. Lett. B 77 (1978) 347.
- [13] H1 Collaboration, A. Aktas et al., Preprint DESY-05-249 (hep-ex/0512060), 2005.
- [14] R. Devenish and A. Cooper-Sarkar, *Deep Inelastic Scattering*. Oxford University Press, 2003.
- [15] ZEUS Collaboration, U. Holm (ed.), *The ZEUS Detector*. Status Report (unpublished), DESY (1993), available on <http://www-zeus.desy.de/bluebook/bluebook.html>.

- [16] N. Harnew et al., Nucl. Inst. Meth. A 279 (1989) 290;
B. Foster et al., Nucl. Phys. Proc. Suppl. B 32 (1993) 181;
B. Foster et al., Nucl. Inst. Meth. A 338 (1994) 254.
- [17] E.N. Koffeman, for the ZEUS MVD group, Nucl. Inst. Meth. A 453 (2000) 89;
D. Dannheim et al., Nucl. Inst. Meth. A 505 (2003) 663.
- [18] M. Derrick et al., Nucl. Inst. Meth. A 309 (1991) 77;
A. Andresen et al., Nucl. Inst. Meth. A 309 (1991) 101;
A. Caldwell et al., Nucl. Inst. Meth. A 321 (1992) 356;
A. Bernstein et al., Nucl. Inst. Meth. A 336 (1993) 23.
- [19] H. Abramowicz et al., Nucl. Inst. Meth. A 313 (1992) 126.
- [20] G. Abbiendi et al., Nucl. Inst. Meth. A 333 (1993) 342.
- [21] J. Andruszków et al., Preprint DESY-92-066, DESY, 1992;
ZEUS Collaboration, M. Derrick et al., Z. Phys. C 63 (1994) 391;
J. Andruszków et al., Acta Phys. Pol. B 32 (2001) 2025.
- [22] M. Helbich et al., Preprint physics/0512153, 2005.
- [23] A.A. Sokolov and I.M. Ternov, Sov. Phys. Dokl. 8 (1964) 1203.
- [24] D.P. Barber et al., Nucl. Inst. Meth. A 329 (1993) 79.
- [25] M. Beckmann et al., Nucl. Inst. Meth. A 479 (2002) 334.
- [26] Polarization 2000 Group, V. Andreev et al., *A Proposal for an Upgrade of the HERA Polarimeters for HERA 2000*, Report DESY PRC 98-07, DESY, 1998.
- [27] G.A. Schuler and H. Spiesberger, *Proc. Workshop on Physics at HERA*,
W. Buchmüller and G. Ingelman (eds.), Vol. 3, p. 1419. Hamburg, Germany, DESY (1991);
H. Spiesberger, *HERACLES and DJANGO: Event Generation for ep Interactions at HERA Including Radiative Processes*, 1998, available on
<http://www.desy.de/~hspiesb/djangoh.html>.
- [28] T. Ishikawa et al., Preprint KEK-92-19, 1993;
F. Yuasa et al., Prog. Theor. Phys. Suppl. 138 (2000) 18.
- [29] L. Lönnblad, Comp. Phys. Comm. 71 (1992) 15.
- [30] G. Ingelman, A. Edin and J. Rathsman, Comp. Phys. Comm. 101 (1997) 108.
- [31] T. Sjöstrand, Comp. Phys. Comm. 39 (1986) 347;
T. Sjöstrand and M. Bengtsson, Comp. Phys. Comm. 43 (1987) 367;
T. Sjöstrand, Comp. Phys. Comm. 82 (1994) 74.
- [32] G. Marchesini et al., Comp. Phys. Comm. 67 (1992) 465.

- [33] H. Jung, *Comp. Phys. Comm.* 86 (1995) 147.
- [34] U. Baur, J.A.M. Vermaseren and D. Zeppenfeld, *Nucl. Phys. B* 375 (1992) 3.
- [35] T. Abe, *Comp. Phys. Comm.* 136 (2001) 126.
- [36] F. Jacquet and A. Blondel, *Proceedings of the Study for an ep Facility for Europe*, U. Amaldi (ed.), p. 391. Hamburg, Germany (1979). Also in preprint DESY 79/48.
- [37] S. Bentvelsen, J. Engelen and P. Kooijman, *Proc. Workshop on Physics at HERA*, W. Buchmüller and G. Ingelman (eds.), Vol. 1, p. 23. Hamburg, Germany, DESY (1992);
K.C. Höger, *Proc. Workshop on Physics at HERA*, W. Buchmüller and G. Ingelman (eds.), Vol. 1, p. 43. Hamburg, Germany, DESY (1992).
- [38] ZEUS Collaboration, M. Derrick et al., *Phys. Lett. B* 316 (1993) 412.
- [39] M. Kataoka, Ph.D. Thesis, Nara Women's University, Report KEK-2005-10, 2005.
- [40] A. Gabareen Mokhtar, Ph.D. Thesis, Tel Aviv University, 2006 (unpublished).
- [41] Particle Data Group, S. Eidelman et al., *Phys. Lett. B* 592 (2004) 1.
- [42] CTEQ Collaboration, H.L. Lai et al., *Eur. Phys. J. C* 12 (2000) 375.
- [43] ZEUS Collaboration, S. Chekanov et al., *Eur. Phys. J. C* 42 (2005) 1.
- [44] J. Pumplin et al., *JHEP* 07 (2002) 012.

ZEUS

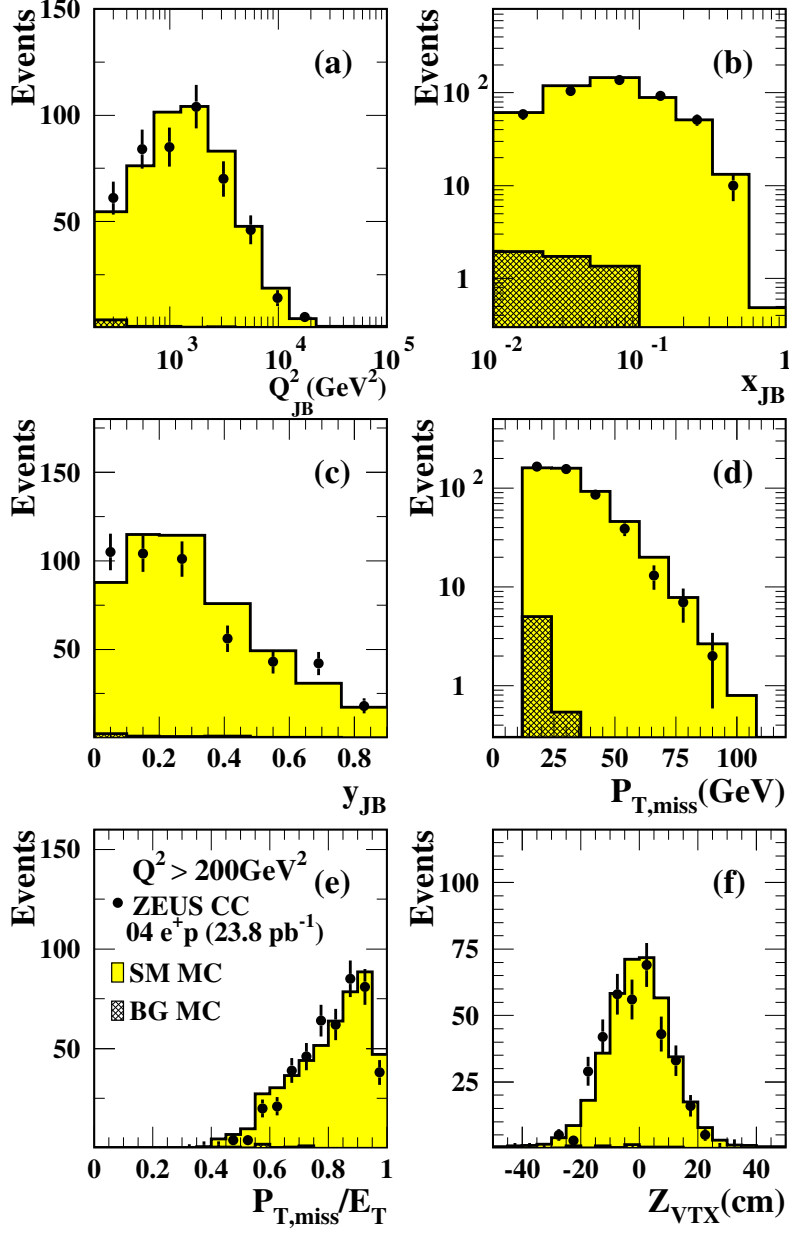


Figure 1: Comparison of the final e^+p CC data sample (solid points) with the sum of the signal and background MC simulations (light shaded histograms). The simulated background events are shown as the dark shaded histograms. The distributions of (a) Q_{JB}^2 , (b) x_{JB} , (c) y_{JB} , (d) $P_{T,\text{miss}}$, (e) $P_{T,\text{miss}}/E_T$ and (f) Z_{VTX} , are shown.

ZEUS

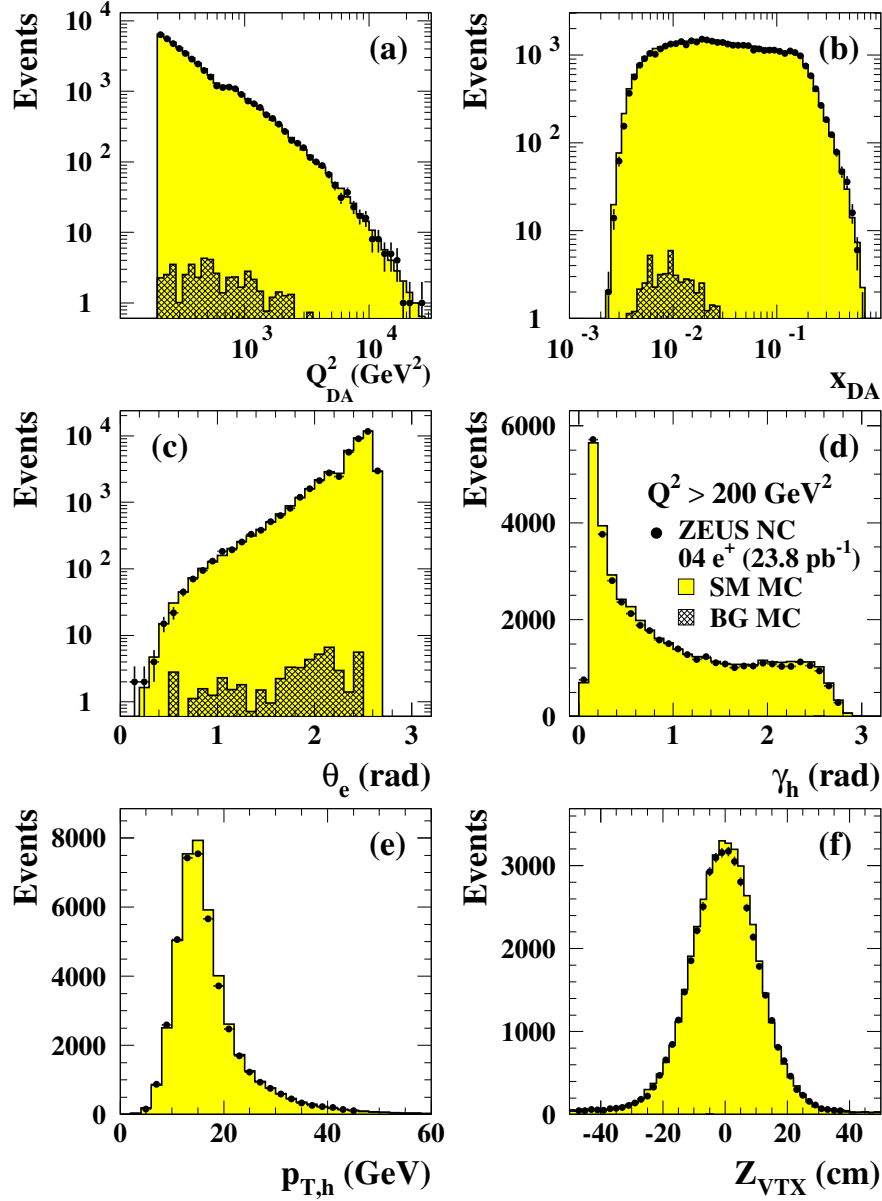


Figure 2: Comparison of the final e^+p NC data sample (solid points) with the sum of the signal and background MC simulations (light shaded histograms). The simulated background events are shown as the dark shaded histograms. The distributions of (a) Q_{DA}^2 , (b) x_{DA} , (c) θ_e , (d) γ_h , (e) $p_{T,h}$, and (f) Z_{VTX} , are shown.

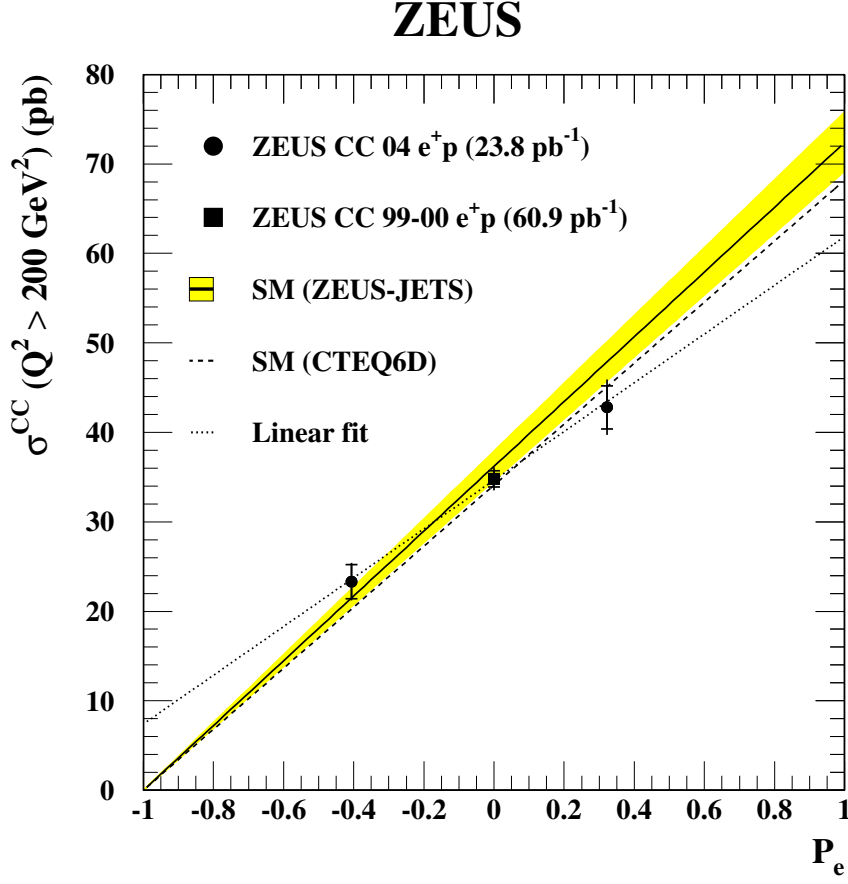


Figure 3: The total cross section for e^+p CC DIS with $Q^2 > 200 \text{ GeV}^2$ as a function of the longitudinal polarisation of the positron beam. The full (dashed) line shows the prediction of the SM evaluated using the ZEUS-JETS (CTEQ6D) PDFs and the shaded band indicates the uncertainty on the cross section from the ZEUS-JETS fit. The dotted line shows the result of the linear fit to the data described in the text. Horizontal error bars representing the uncertainty on the measured polarisation are included but are too small to be visible.

ZEUS

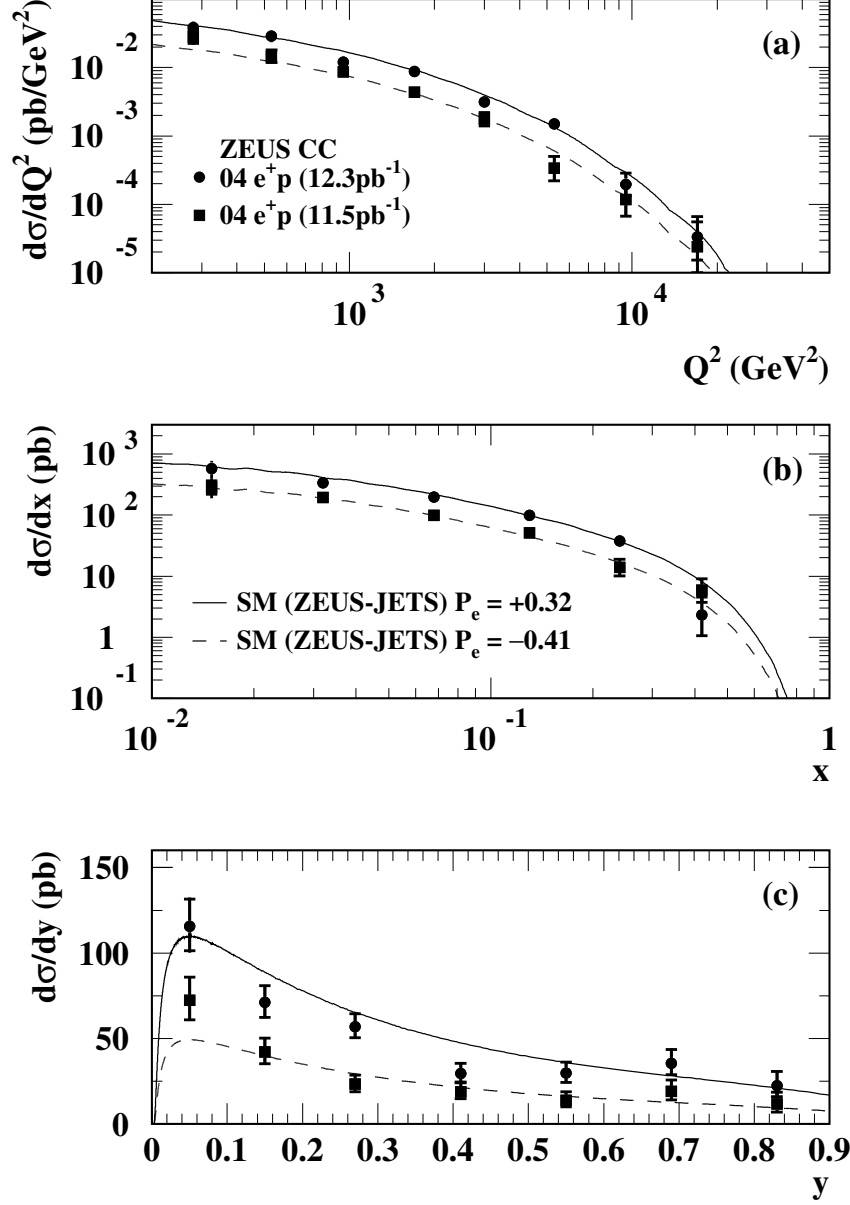


Figure 4: The e^+p CC DIS cross-sections (a) $d\sigma/dQ^2$, (b) $d\sigma/dx$ and (c) $d\sigma/dy$. The circles (squares) represent data points for the positive (negative) polarisation measurements and the curves show the predictions of the SM evaluated using the ZEUS-JETS PDFs.

ZEUS

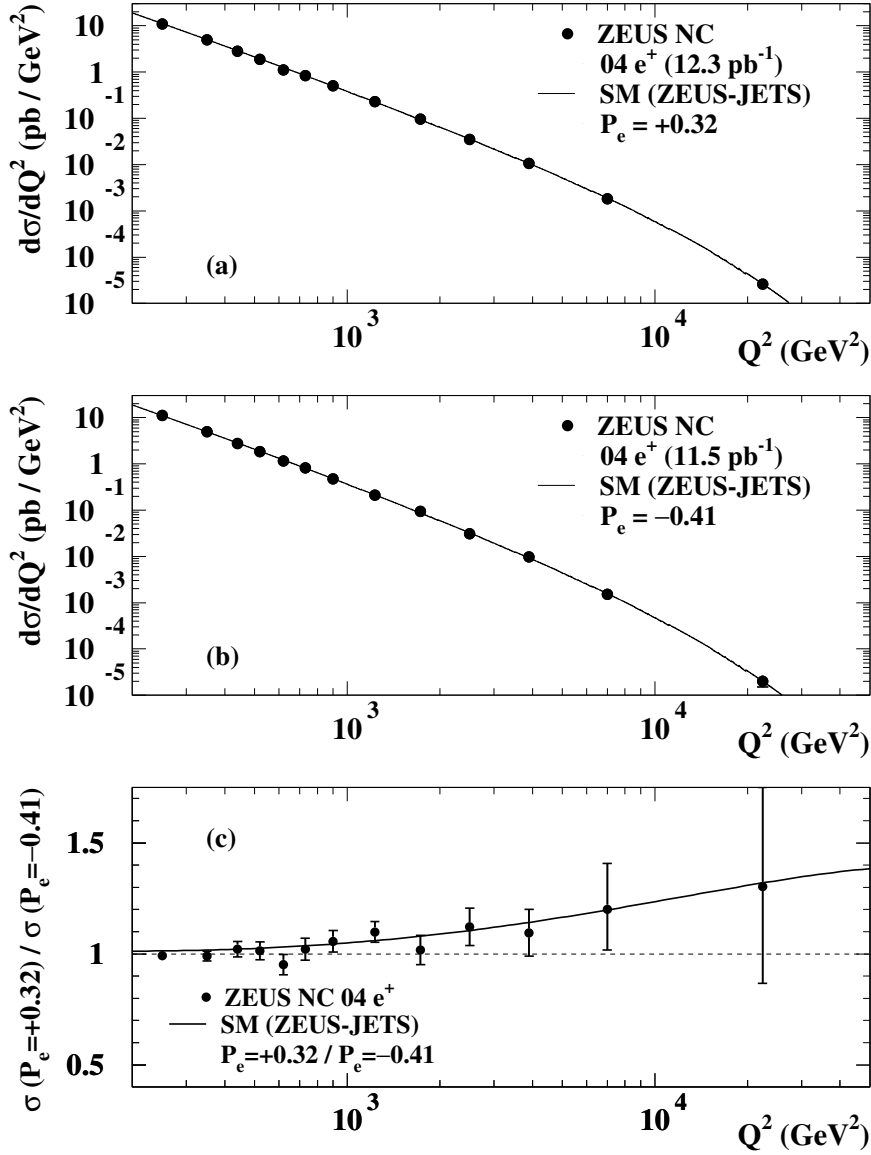


Figure 5: The e^+p NC DIS cross-section $d\sigma/dQ^2$ for (a) positive polarisation data, (b) negative polarisation data and (c) the ratio of the two. The full lines show the predictions of the SM evaluated using the ZEUS-JETS PDFs and the dashed line the prediction with no dependence on the longitudinal polarisation of the positron beam.